A MEMS VIBRATING BEAM ACCELEROMETER FOR HIGH RESOLUTION SEISMOMETRY AND GRAVIMETRY

Guillermo Sobreviela-Falces[1,2], Milind Pandit[1,2], Arif Mustafazade[1,2], Chun Zhao[1], Callisto Pili[2], Colin Baker[2] and Ashwin Seshia[1,2]

[1] Nanoscience Centre, Department of Engineering, University of Cambridge, UK. and
[2]Silicon Microgravity Ltd., Cambridge Innovation Park, Waterbeach, Cambridge, UK

ABSTRACT

A differential MEMS vibrating beam accelerometer (VBA) demonstrating excellent stability for seismology and gravimetry applications is presented. The accelerometer response demonstrates excellent linearity over an acceleration range of ±1 g (1 g = 9.8 m s^{-2}) with a scale factor of 9825 Hz/g. An approximately flat output Allan deviation with an average value of 15 ng is recorded over integration times τ= 1 s – 1000 s with a best-case bias instability of < 10 ng and a noise floor of 10 ng/√Hz. These results, taken collectively, set new benchmarks for vibrating beam MEMS accelerometers.

KEYWORDS

Micromechanical devices, resonators, thermal stability, frequency stability, sensors.

INTRODUCTION

MEMS accelerometers are increasingly being adopted in applications where high performance is required, including inertial navigation [1], seismometry [2] and gravimetry [3]. Silicon MEMS VBAs have been researched for several decades in this context [4]–[12]. Improvements in the in-chip vacuum-packaging [12] and temperature compensation and control [13] of the MEMS device has enabled the VBA approach to meet requirements for navigation-grade inertial measurement systems [14] and the tracking of Earth tides and recording of tele-seismic events [12].

In this paper, a new generation MEMS VBA is presented building upon previous work. A description of the MEMS technology and results from initial experimental characterization of the sensor module is provided. A combination of advances in design, packaging, interface electronics and thermal control enable the significant advances in noise floor and stability. An outstanding low bias instability with a best-case value of 7 ng @ 900s (average value of 15 ng over integration times τ = 1 s – 1000 s) and a noise floor of 10 ng/√Hz is demonstrated.

MEMS DEVICE

MEMS Design

The differential vibrating beam MEMS accelerometer is fabricated in a SOI-based process employing wafer-level vacuum encapsulation [12]. The device is composed of the four classic elements of the VBA [4]: the inertial mass, suspensions, levers (force amplification of 30), anchors, and the resonator/s. This structure also includes two comb-drive arrays at the mass endings for self-test purposes.

A schematic view of the silicon MEMS device is shown in Fig. 1a, and an optical image of the suspension and the system lever-resonators can be seen in Fig. 1 b-c, where the images have been colored following the scheme of Fig. 1a.

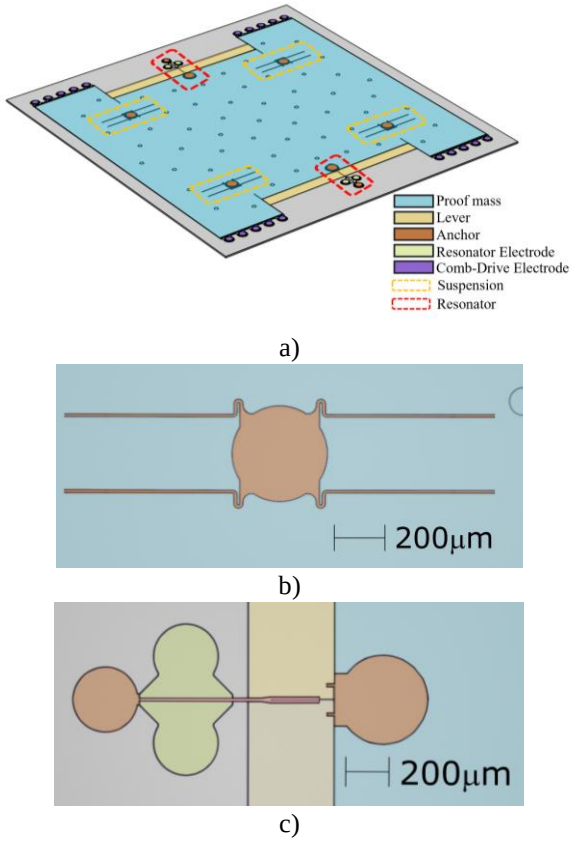

Figure 1: 3D model of the 10.3 mm by 9.7 mm differential vibrating MEMS accelerometer: a) General overview. Optical images of b) Suspension. c) Lever-resonator system.

MEMS Packaging

Wafer-level vacuum encapsulation of the MEMS resonator is achieved through fusion bonding of wafers under vacuum as previously outlined [12]. The vacuum package of the device allows high quality factors (25000) limited by thermoelastic damping in the single-crystal silicon resonator. The MEMS chip is attached to a leadless ceramic chip carrier using a low stress die attach adhesive. Electrical packaging is completed using wire-bonding and die-level encapsulation (See Fig.2). The chip is designed to be actively temperature controlled to a desired set-point to minimize temperature sensitivity of the response.

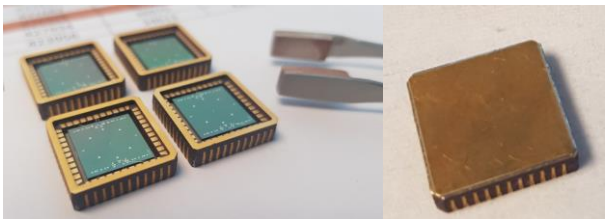

Figure 2: a) Ceramic chip carrier containing the MEMS device. b) Ceramic chip carrier following die-level encapsulation.

Electrical Interface

The electrical interface is divided in two parts: Analog and Digital. The analog part is connected to the actuation and read-out electrodes of the resonator. The input of each resonator is actuated by a sinusoidal signal generated at by the DAC output of a DRTU (Digital Resonance Tracker Unit). The output signal of each resonator is amplified by a transimpedance amplifier (TIA) with an equivalent input noise of 50 fA/√Hz and a 100 MΩ transimpedance gain @ 270 kHz.

The output of the TIA stage is connected to the DRTU where the signal is digitized. Following this, the signal is processed for any of both uses: The open loop characterization of the resonators or closed-loop actuation under PLL control. The digital interface is implemented in a commercial Xilinx Zynq Z7020 FPGA operating with a sampling rate of 40 Msps. Figure 3 shows the Analog-Digital electrical interface diagram for one of the MEMS resonators. Each resonator channel has its own autonomous DRTU system, sharing only the CPU and Memory Configuration Map of the FPGA.

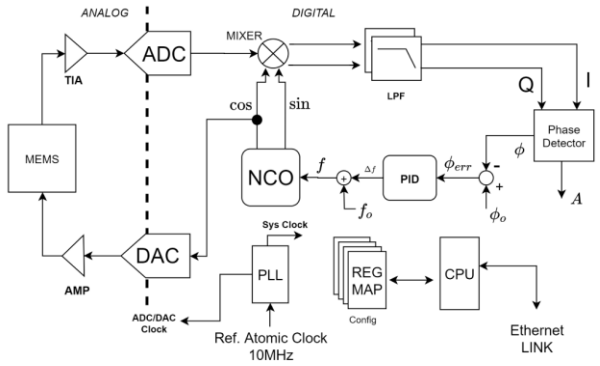

Figure 3: Digital Resonance Tracker Unit, (single resonator view)

Open-loop response

The open-loop frequency response of the resonators when the sensing axis of the device is oriented in a vertical position (1 g acceleration) is shown in Fig. 4. The open loop measurements are first performed with a Zurich Instrument MFLI Lock-in amplifier and secondly using the implemented DRTU for comparison with both measurements demonstrating good agreement. The frequency values are 261.9 kHz and 270.5 kHz, and the extracted Q-factor of the resonances is approximately 26000 and 27000, respectively. The linearity of the resonance allows a maximum output amplitude of 185 mV before exhibiting a nonlinear hardening effect [15].

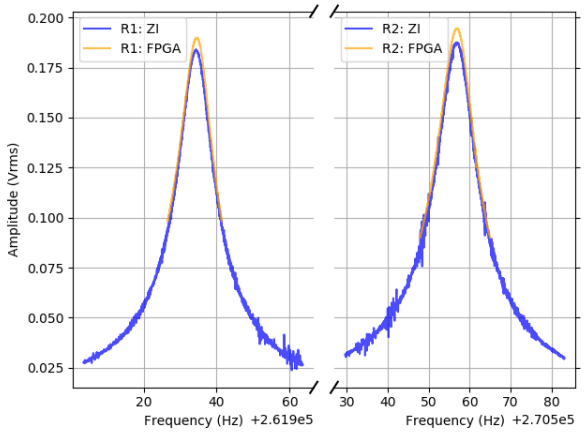

Figure 4: Measured open-loop response of the resonators.

Closed-loop response

The DRTU system is used to operate each one of the resonators in an independent closed loop, tracking the resonance frequency of each resonator. The PLL parameters of each one of these loops are set to: PLL Bandwidth of 1Hz, an input filter bandwidth of 5Hz (composed by three 2nd order biquad filters), and a filter loop sampling rate of 16ksps.

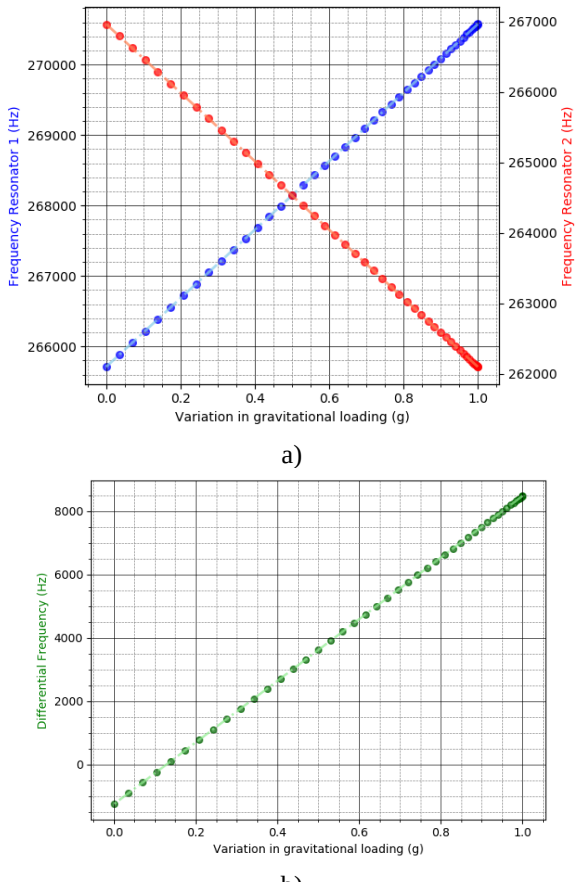

Figure 5: Results of scale factor characterization demonstrating the variation in a) individual resonance frequencies, b) differential frequency with changes in gravitational loading along the sensitive axis.

The closed-loop response of the sensor to variation in gravitational loading is characterized using a tilt table with

1-degree angular positioning resolution. The sensitive axis of the chip is aligned to specific angles relative to the vertical in this experiment. Figure 5.a shows the resonators frequency response for a set of accelerations from 0 to 1 g, produced by a tilt from 0 to 90 degrees with an angular step of 2 degrees. Figure 5.b shows the differential response of the differential VBA, demonstrating a scale factor of 9825 Hz/g with excellent linearity over the ±1 g range.

SYSTEM ENVIRONMENTAL CONTROL

The system is designed with a two-stage temperature control implement. In both cases, a heating element controlled by an independent PID loop is implemented. The first level contains the ceramic chip carrier and the MEMS device. The second module level control accommodates both the MEMS chip and the VBA front-end electronics (Transimpedance amplifier, voltage regulators, filters).

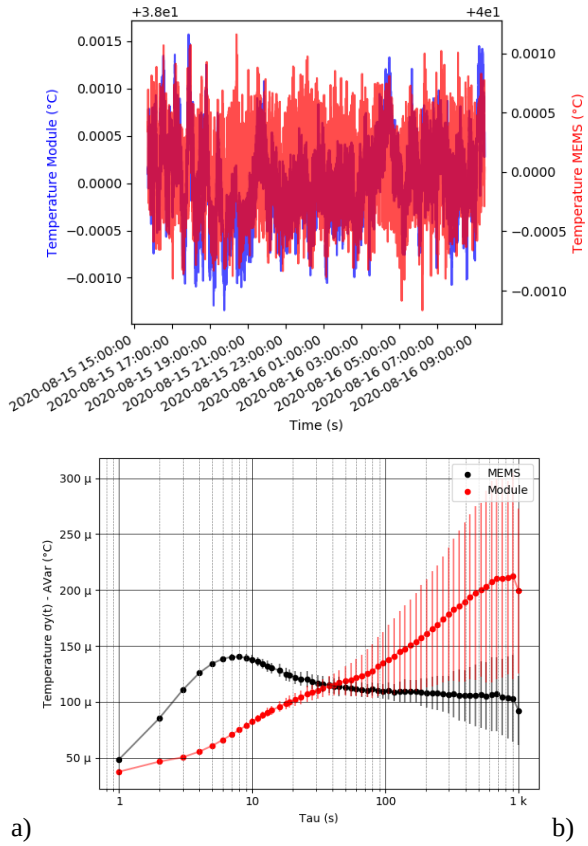

Figure 6: a) Recorded temperature during a time span of 18 hours. b) Temperature stability (Allan Variance) of the system for 18 hours analyzed in data chunks of 10000 s. The solid line corresponds to the average value of Allan variance and a standard deviation indicating run-to-run variability is provided.

The MEMS chip temperature is maintained at 40°C, while the second module-level is kept at 38°C for these experiments though these set points can be tuned for practical applications. As seen in Fig.6, the two-stage temperature control ensures an extremely stable environment characterized by a temperature bias stability on the MEMS and the module of 100 µ°C and 200 µ°C @ τ = 1000s, respectively.

SENSOR CHARACTERIZATION

The sensor module is then adapted for closed-loop continuous recording measurements. These measurements are conducted synchronously with the temperature measurements reported in Fig. 6. The differential frequency output of the VBA demonstrates a linear drift of approximately 350 µHz/hour, equivalent to 35.6 ng/hour which can be corrected for in software. The Allan deviation of the sensor output, in acceleration units, is shown in Fig 7.a and Fig 7.b plots the input-referred power spectral density. The system exhibits a flat bias stability with an average bias stability of 15 ng (τ = 1 s – 1000 s) and a 10 ng/√Hz noise floor. It is possible to distinguish seismic noise in the power spectral density at the frequencies of 400 mHz and 2 to 5 Hz, which make an appearance during the daytime between 8AM – 18PM (see orange line) and disappear during night (see blue line).

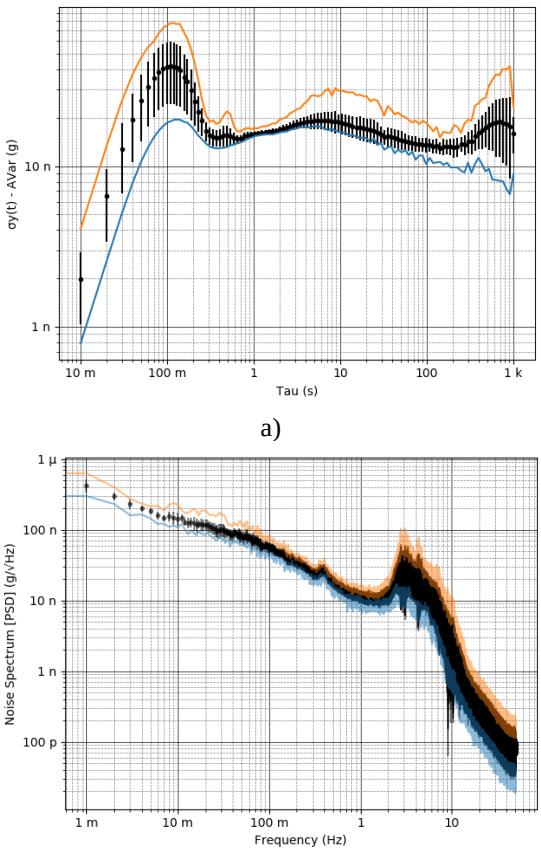

Figure 7: Analysis of the output response of the VBA. Stability analysis of the VBA output signal during the dates 2020-8-15 @ 15:00 to 2020-8-16 @ 9:00 (Analysis performed over a total time length of 18 hours using 10000-second-long segments). The best stability segment is plotted in blue, the worst stability segment in orange and the average stability values with the corresponding error vars is plotted in black. a) Allan variance calculation. b) Accelerometer noise power spectral density.

The specific values of bias instability and noise floor for the presented MEMS VBA are compared with previous work in table I, demonstrating the performance evolution

achieved over the years. The improvements reported in this work arise from a combination of features including an increased scale factor, improvements in packaging and further optimization of the interface electronics and thermal control of the chip and sensor module.

Table 1: State-of-the-art comparison of noise floor and bias instability for the MEMS VBA

Work / Year	Noise Floor (ng/√Hz)	Bias instability (ng)
[7] 2017	1000	230
[8] 2017	N/A	160
[9] 2015	150	N/A
[10] 2017	380	95
[11] 2019	98	56
[12] 2020	100	9
This work	10	7

CONCLUSION

In this work, a differential MEMS VBA is presented for low-noise, high stability measurements. This is achieved through considered co-optimization of the MEMS chip, package, readout electronics, and thermal control systems. The prototype module achieves a noise floor of 10 ng/√Hz and a bias instability of 7 ng @ τ = 900s, representing the best results recorded to-date using a MEMS VBA. The module is currently being adapted for surface gravity field trials in the UK.

ACKNOWLEDGEMENTS

Support from Innovate UK and the Cambridge Centre for Smart Infrastructure and Construction is gratefully acknowledged.

REFERENCES

[1] P. Zwahlen, A.-M. Nguyen, Y. Dong, F. Rudolf, M. Pastre, and H. Schmid, "Navigation grade MEMS accelerometer," in Proc. IEEE 23rd Int. Conf. Micro Electro Mech. Syst. (MEMS), Sep. 2010, pp. 631–634.

[2] W. T. Pike, I. M. Standley, S. B. Calcutt, and A. G. Mukherjee, "A broadband silicon microseismometer with 0.25 ng/rthz performance," in Proc. IEEE Micro Electro Mech. Syst. (MEMS), Jan. 2018, pp. 113–116.

[3] R. Middlemiss, A. Samarelli, D. Paul, J. Hough, S. Rowan, and G. Hammond, "Measurement of the earth tides with a mems gravimeter," Nature, vol. 531, no. 7596, p. 614, Mar. 2016.

[4] A. A. Seshia et al., "A vacuum packaged surface micromachined resonant accelerometer," J. Microelectromech. Syst., vol. 11, no. 6, pp. 784–793, Dec. 2002.

[5] C. Comi, A. Corigliano, G. Langfelder, A. Longoni, A. Tocchio, and B. Simoni, "A resonant microaccelerometer with high sensitivity operating in an oscillating circuit," J. Microelectromech. Syst., vol. 19, no. 5, pp. 1140–1152, Oct. 2010.

[6] X. Zou, P. Thiruvenkatanathan, and A. A. Seshia, "A seismic-grade resonant MEMS accelerometer," J. Microelectromech. Syst., vol. 23, no. 4, pp. 768–770, Aug. 2014.

[7] J. Zhao et al., "A 0.23 μg bias instability and 1μg/hz1/2 acceleration noise density silicon oscillating accelerometer with embedded frequencyto-digital converter in pll," IEEE J. Solid-State Circuits, vol. 52, no. 4, pp. 1053–1065, Sep. 2017.

[8] D. D. Shin, C. H. Ahn, Y. Chen, D. L. Christensen, I. B. Flader, and T. W. Kenny, "Environmentally robust differential resonant accelerometer in a wafer-scale encapsulation process," in Proc. IEEE 30th Int. Conf. Micro Electro Mech. Syst. (MEMS), Jan. 2017, pp. 17–20.

[9] X. Zou and A. A. Seshia, "A high-resolution resonant mems accelerometer," in Proc. 18th Int. Conf. Solid-State Sensors, Actuat. Microsyst., Jun. 2015, pp. 1247–1250.

[10] Y. Yin, Z. Fang, F. Han, B. Yan, J. Dong, and Q. Wu, "Design and test of a micromachined resonant accelerometer with high scale factor and low noise," Sens. Actuators A, Phys., vol. 268, pp. 52–60, Dec. 2017.

[11] C. Zhao, M. Pandit, G. Sobreviela, P. Steinmann, A. Mustafazade, X. Zou, A. A. Seshia, "A Resonant MEMS Accelerometer With 56ng Bias Stability and 98ng/Hz 1/2 Noise Floor," J. Microelectromech. Syst. 2019, 28, 324–326.

[12] A. Mustafazade et al., "A vibrating beam MEMS accelerometer for gravity and seismic measurements," Scientific Reports, vol. 10, no. 10415, June. 2020.

[13] A. Mustafazade and A. A. Seshia, Compact High-Precision Analog Temperature Controller for MEMS Inertial Sensors, Proc. 2018 IEEE Intl. Freq. Control Symposium, 2018.

[14] O. Lefort, I. Thomas, S. Jaud, "To the production of a robust and highly accurate MEMS vibrating accelerometer. In Proceedings of the 2017 DGON Inertial Sensors and Systems (ISS), Karlsruhe, Germany, 19–20 September 2017.

[15] G. Sobreviela et al. "Suppression of the af-mediated noise at the top bifurcation point in a mems resonator with both hardening and softening hysteretic cycles," Sensors and Actuators A: Physical, 2017.